Quantum topology identification with deep neural networks and quantum walks

Yurui Ming,[1] Chin-Teng Lin,[1] Stephen D. Bartlett,[2] and Wei-Wei Zhang[2,*]

[1] *Centre for Artificial Intelligence, School of Software, University of Technology Sydney, Sydney, Australia*

[2] *Centre for Engineered Quantum Systems, School of Physics, The University of Sydney, Sydney, Australia*

(Dated: December 3, 2018)

Topologically ordered materials may serve as a platform for new quantum technologies such as fault-tolerant quantum computers. To fulfil this promise, efficient and general methods are needed to discover and classify new topological phases of matter. We demonstrate that deep neural networks augmented with external memory can use the density profiles formed in quantum walks to efficiently identify properties of a topological phase as well as phase transitions. On a trial topological ordered model, our method's accuracy of topological phase identification reaches 97%, and is shown to be robust to noise on the data. Our approach is generally applicable and may be used for topology identification with a variety of quantum materials.

Introduction

The properties of topological quantum materials have been the subject of intense interest in recent years, due to their paradigm-changing implications for condensed matter physics [1–4] and potential applications to new technologies. The electric conductivity of topological materials such as topological insulators has potential applications for magnetoelectric devices with higher efficiency and lower energy consumption [6–8]. In addition, topological materials can support anyonic quasiparticle excitations, with exotic statistics under braiding transformations that may enable fault-tolerant quantum computing [5, 9]. The topological ordering of quantum materials can be characterised with quantised, nonlocal topological invariants, such as the Chern number of the quantum Hall effect. These invariants determine all of the key topological properties of quantum systems, such as the number of topological edge states. The discovery and characterisation of novel topological quantum materials requires a general and efficient method to identify these topological invariants. For bulk systems, these can generally be inferred from the existence of edge states [2, 10], or particle dynamics, such as the anomalous velocities obtained by wave packets under applied forces [11, 12], and quantum walks [13–18]. While there has been considerable theoretical progress in developing classification methods for topological phases, we still lack a universal automatic method for the discovery and characterisation of new materials.

Here we propose and test a universal automated method for identifying topological phases of quantum materials, combining quantum walks to probe the phase and a deep neural network (DNN) to analyse the evolution. Using the particle density profiles formed during a particle's evolution driven by the system's Hamiltonian, we demonstrate that a novel DNN with external memory is able to identify the topological phases and phase transitions for a two-dimensional lattice model with spin-orbit coupling. Our method demonstrates high identification accuracy, greater than 97%, and is robust to noise on the input data. Our results provide a powerful tool for the efficient discovery and analysis of novel topological quantum systems, and therefore the design of robust quantum technologies.

Results

Continuous-time quantum walks in topological quantum systems. The coherent dynamics of particles, with motion dependent on an internal degree of freedom such as spin, are described as quantum walks. Along with providing an advanced tool for building quantum algorithms, quantum walks also provide a platform to simulate and analyse complex physical systems [20]. Discrete-time quantum walks have been shown to be closely related with the topology of the driving system. The experimental observations of particle localisation at the boundary between materials possessing different topological ordering and its robustness to the defects have been used to prove the existence of topologically protected edge modes [13–16, 21, 22]. The moments of the probability distribution for the walker's position after many steps is an experimental signature of a topological quantum phase transition in one-dimensional quantum walks [15]. Continuous-time quantum walks (CTQW) with a two-dimensional spin-orbit lattice Hamiltonian can also reveal topological phase transitions [17], a fact supported by recent experiments [18]. In such CTQW, the resulting density profile of an initially localized particle is expected to contain a wealth of information to identify the topological order of the underlying quantum system, provided one can extract this information efficiently.

The topological phases we consider are described by a parameterised Hamiltonian on a two-dimensional lattice (599×599 in our simulation). Following Ref. [17], we use a continuous-time quantum walk (CTQW) for a initially localised single particle under this Hamiltonian, where the behaviour of the distribution of the quantum state after long times provides a signature of the topological phase. We will investigate the use of both the particle's spatial distribution $p(x, y)$ as well as its momentum space distribution $p(k_x, k_y)$, marginal-

*Electronic address: ww.zhang@sydney.edu.au

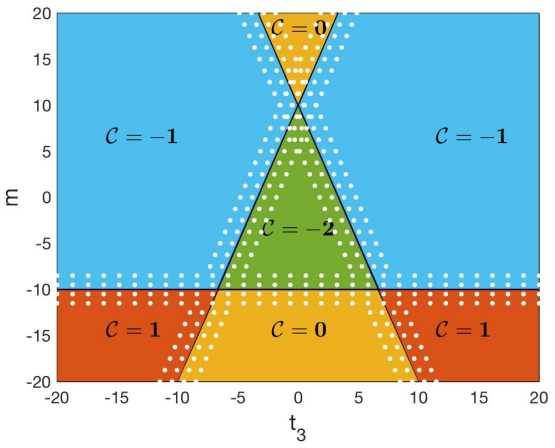

FIG. 1: The parameter space of the Hamiltonian of Eq. (2) with fixed $t_{1x} = t_{1y} = 1$, $t_2 = 5$, used for the generation of our dataset. The coloured regions represent the "whole" areas, and the dotted regions are the "transition" areas, as detailed in Table I. A parameter space containing the phase $\mathcal{C} = +2$ is similar, with this phase located at the same region of $\mathcal{C} = -2$, obtained by flipping the sign of t_{1y} and keeping the other parameters the same.

izing over the particles internal state. Specifically, we consider the two-dimensional spin-orbit lattice Hamiltonian [17, 18, 39, 40], described in the Methods. We use this model to test our method for topological phase identification because the topological invariant (Chern number) of this system is easily calculated. This Hamiltonian supports five distinct topological phases, labelled by the Chern number $\mathcal{C} \in \{0, \pm 1, \pm 2\}$, determined by the coupling parameters in this Hamiltonian, as shown in Fig. 1.

The density profile is strongly dependent on the system's topology, and can be used as a diagnostic of topological phases, and the phase transitions between them, as discussed in Refs. [17, 18]. From these previous studies, good signatures for topological phase identification are the central features of the position distribution and the ring pattern of the momentum distribution, which reveal that the Hamiltonian localizes in a nontrivial topological phase with Chern number $\mathcal{C} = \pm 1$. However, these previous analyses are based on approximations, and we do not have a general method to analyse the density profiles for topological phases associated with other Chern numbers.

Learning topological phases using a deep neural network. Machine learning can determine the underlying characteristics of a physical system even without prior human knowledge [23]. Deep learning, a subset of machine learning which represents the data as a nested hierarchy of concepts, provide great capability and adaptability in this regard. Each concept is defined in relation to simpler concepts, and more abstract representations are computed in terms of less abstract ones. Deep learning has achieved breakthroughs across many applications [24–26], indicating its potential benefit in the analysis of many different quantum problems [27–36]. Inspired by the hierarchical biostructures in vision systems [37], deep neural networks (DNN) can automatically extract the most suitable representations from input data and make accurate predictions. Generally speaking, during the end-to-end learning process, the representations of data will emerge rather than being discovered or manually crafted [38].

We will apply DNN to the problem of topological identification by providing the network with the density profiles from a CTQW as input. As described above, the density profiles contain a wealth of information about the topological phase of the system, but identifying which features are important is challenging, especially for higher order phases. A DNN with external memory has the capacity to solve complex, structural tasks that are inaccessible to stand-alone neural networks, and has shown the ability to answer synthetic questions designed to emulate reasoning and inference problems [41]. The architecture of our deep neural network is shown in Fig. 2, which consists of multiple computation blocks (CB) and fully connected layers (computation network), as well as an external memory coupled to the last convolutional layer (memory network). The computation network is of a supervised-learning paradigm and the memory network is of an unsupervised-learning paradigm. Both are jointly trained during the process.

Our experiment consists of four steps: data preparation, neural network training, validation, and testing. The data preparation stage is based on numerically simulations of CTQW with different Hamiltonian parameters, and is described in the Methods. The data corresponding to different topological phases is randomised and split into three sets with the ratio 0.8 : 0.1 : 0.1 for training, validation and testing respectively. The prepared data is reused three times to evaluate the network. As the performance indicator for the corresponding prepared data, the accuracy in our results is the average over three independent randomisation sets.

We illustrate the outcome of our experiments using the principal component analysis (PCA) of memory, a t-distributed stochastic neighbour embedding (t-SNE) of the computation network output, and the statistical accuracy of the test. Both the PCA and the t-SNE are visualisation results, and the accuracy is a statistical evaluation. The t-SNE shows the topological classification of input data corresponding to different Chern numbers. The PCA demonstrates how the input data is clustered according to its correlation by self-organisation, which distinguishes the different topological phases of the input data. The accuracy shows the identification accuracy calculated from the test data.

The PCA and t-SNE based on the data—the density profiles in momentum and position space—are shown in Fig. 3, where the DNN identification forms separated clusters associated with the five topological phases of our model Hamiltonian system. For the momentum space data, the identification clearly reveals five clusters corre-

sponding to each of the distinct topological phases of the Hamiltonian. For the position space data, only four clusters are identified; the topological phases corresponding to Chern numbers $\mathcal{C} = \pm 2$ are not distinguished based on this data.

The statistical accuracy of our test, i.e., the ratio between the number of testing samples classified into correct topological phases and the total number of testing samples, is shown in Table I. We see that, when based on momentum space distributions, we obtain a very high accuracy for data covering both the whole phase diagram region and a restriction to the region around the phase transition (97% and 91.7% respectively). Position space distributions lead to identification with relatively lower accuracy for the same regions (70.3% and 71.4% respectively), especially for the case $\mathcal{C} = 2$. The unbalanced accuracies for $\mathcal{C} = -2$ and $\mathcal{C} = 2$ cases are likely due to the relatively smaller region for $|\mathcal{C}| = 2$ in our phase diagram of Fig. 1. The relatively low accuracy for data in position space indicated the data in position space is less directly connected with the Chern number of the Hamiltonian as defined in Eq. (3). As the density profiles in position and momentum spaces are directly related to each other via the Fourier Transformation, and so fundamentally carry the same information, we conjecture that to obtain a higher accuracy with position density profiles as input data a much larger size of DNN is required to compensate the Fourier Transformation of the information, and data augmentation will also help [42–44] as discussed below.

Noisy data as input. Quantum walks on engineered topological quantum materials have been realised in different physical platforms including photonics systems [14, 19, 22, 46] and cold atoms [18], amongst others. For our method to be useful on experimental data, it must be robust to noise. Here, we test the performance of our method with noisy input data for our trained DNN. We add Gaussian noise to our simulated data, at a level comparable with current experimental techniques in optical systems [22, 46] and cold atoms systems [10, 18, 45]; details are discussed in the *Methods*.

In these tests, the accuracy statistics for topological phase identification shows limited degradation as indicated in Table I. We can see that the accuracy only drops 0.020 on average with momentum density profiles, which could potentially be offset by increasing the size of the network. One unexpected outcome is that, with noise on the density profiles in position space, the accuracy is 0.008 and 0.030 higher that the accuracy obtained with the data without noise. The performance increase with noise data in position space is potentially due to the effect of a data augmentation for training deep neural network [42–44]. The Gaussian noise introduced in our data increases the margin of the decision boundary, given an accuracy of around 70%.

Conclusion and outlook.

We have demonstrated a universal automatic method for the identification of distinct topological phases of quantum materials. Our simulated experimental results show that the combination of the particle's density profile from a CTQW and DNN augmented with external memory is a reliable and efficient method to identify topological phases and phase transitions in our trial system, even for the high order $\mathcal{C} = \pm 2$ and noisy data. Our approach is generally applicable and may be used for the identification of topological phases with a variety of quantum materials.

Methods

Here we present the trial topological Hamiltonian system, and describe the generation of a particle's density profile as used as the input data for our DNN. We also provide the details of the architecture of our DNN.

The topological system in our simulated experiments. The two-dimensional spin-orbit lattice Hamiltonian we consider here is [17, 18, 39, 40]

$$\begin{aligned}\hat{H} = \sum_{x,y} \Big[& c^\dagger_{x,y} \frac{m}{2} \hat{\sigma}_3 c_{x,y} + c^\dagger_{x+1,y}(t_{1x}\hat{\sigma}_1 - \mathrm{i}t_3\hat{\sigma}_3)c_{x,y} \\ & + c^\dagger_{x,y+1}(t_{1y}\hat{\sigma}_2 - \mathrm{i}t_3\hat{\sigma}_3)c_{x,y} + c^\dagger_{x+1,y+1} t_2 \hat{\sigma}_3 c_{x,y} \\ & + h.c.\Big] \\ = & \sum_{k_x,k_y} \vec{h}\cdot\vec{\sigma}\,|k_x,k_y\rangle\langle k_x,k_y|\,, \end{aligned} \tag{1}$$

using $\{m, t_{1x}, t_{1y}, t_2, t_3\}$ as the coupling parameters, $i \in \{1,2,3\}$, $\vec{\sigma} = \{\hat{\sigma}_1, \hat{\sigma}_2, \hat{\sigma}_3\}$ as the Pauli operators and $\vec{h} = (h_1, h_2, h_3)$. The last line of Eq. (1) is obtained by using translation invariance and the Fourier Transformation $\{|k_x\rangle = \frac{1}{\sqrt{2\pi}}\sum_x e^{-ixk_x}|x\rangle, |k_y\rangle = \frac{1}{\sqrt{2\pi}}\sum_y e^{-iyk_y}|y\rangle\}$, the 2×2 block diagnosed Hamiltonian in momentum space is

$$\begin{aligned}\vec{h}\cdot\vec{\sigma} = & 2t_{1x}\cos k_x\hat{\sigma}_1 + 2t_{1y}\cos k_y\hat{\sigma}_2 \\ & + \{m + 2t_3(\sin k_x + 2\sin k_y) \\ & + 2t_2\cos(k_x + k_y)\}\hat{\sigma}_3\,. \end{aligned} \tag{2}$$

This Hamiltonian supports the topological phases with $\mathcal{C} \in \{0, \pm 1, \pm 2\}$ by varying the coupling parameters m, t_3 while fixing $t_{1x} = t_{1y} = 1, t_2 = 5$, with the definition of Chern number as

$$\mathcal{C} = \frac{1}{4\pi}\int_{\mathrm{BZ}} d^2\mathbf{k}\;\hat{h}\cdot\left(\partial_{k_x}\hat{h}\times\partial_{ky}\hat{h}\right)\,, \tag{3}$$

with $\hat{h} = \vec{h}/|\vec{h}|$ [39]. The different topological phases labelled by Chern number $\mathcal{C}$, as a function of Hamiltonian parameters, is shown in Fig. 1.

The formation of particle's density profile in both momentum and position spaces. In CTQW evolutions, a particle with spin up, initially localised in the centre of a two-dimensional lattice in position space, spreads out and gradually occupies a larger area of the lattice. Equivalently, the particle is initially uniformly distributed in momentum space and during the evolution the particle's components at every momenta oscillates between spin

up and spin down components. The particle's probability distributions in both position and momentum spaces form a certain pattern which is closely related with the Hamiltonian.

At evolution time t, the state of the particle initially localised at the centre of two-dimensional lattice is (setting $\hbar = 1$)

$$\begin{aligned} |\psi(t)\rangle &= \sum_{\boldsymbol{k}} \left(\alpha_{\boldsymbol{k}\uparrow} |\uparrow\rangle + \alpha_{\boldsymbol{k}\downarrow} |\downarrow\rangle\right) |\boldsymbol{k}\rangle \\ &= \sum_{\boldsymbol{k}} \begin{pmatrix} \frac{h_3(-\mathrm{isin}(E_{\boldsymbol{k}}t))}{E_{\boldsymbol{k}}} - \cos\left(E_{\boldsymbol{k}}t\right) \\ \frac{(h_1+\mathrm{i}h_2)(-\mathrm{isin}(E_{\boldsymbol{k}}t))}{E_{\boldsymbol{k}}} \end{pmatrix} |\boldsymbol{k}\rangle \end{aligned} \quad (4)$$

where $E_{\boldsymbol{k}} = \sqrt{h_x^2 + h_y^2 + h_z^2} \neq 0$ is the eigenenergy of system's Hamiltonian. When $E_{\boldsymbol{k}} = 0$ we have $\alpha_{\boldsymbol{k}\uparrow} = 1$ and $\alpha_{\boldsymbol{k}\downarrow} = 0$, which is the case at Dirac point while the system is under topological phase transition. The particle's state represented in position space is the Fourier transform of the corresponding spin components.

From the expression of Eq. (4) for particle's state at time t, the amplitude and the relative phase of both spin up and spin down components are closely related with the energy $E_{\boldsymbol{k}}$ and sensitive to the band gap of the system which is $\min\{2E_{\boldsymbol{k}}\}$ as discussed in Ref. [17, 18]. The topological phase of the system characterised with Chern number is revealed by the band structure of the system. Therefore, the particle's density profile is a competitive candidate for the topological detection, even for higher order phases.

Here, we generate two sets of density profiles. One is in momentum space and the other is in position space. For the training of the neural network, we decompose the complex values of both spin up and spin down components into two real values and map the amplitude and relative phase matrices into image representation. With this process, the input data set consists of the set of spatial or momentum distributions for the particle's final states.

Dataset generation for our deep neural network identifying the topology of quantum matters. Our system supports topological phases with $\mathcal{C} = \{0, \pm 1, \pm 2\}$ as described above. The diagram showing the distribution of Chern number $\mathcal{C}$ with respect to m, t_3 and fixed $t_{1x} = t_{1y} = 1, t_2 = 5$ is shown in Fig. 1, where the shaded area represents the parameter area for the dataset labeled as "whole" and the dotted area represents the parameter area for the dataset labeled as "transition" in our tables. The dataset for $\mathcal{C} = 2$ is generated with the same m, t_3, t_{1x}, t_2 as $\mathcal{C} = -2$, but with $t_{1y} = -1$. The sizes of our dataset generated for the whole phase diagram are $\{1449, 1478, 1486, 1488, 1449\}$ and for the phase transition area of the diagram are $\{2542, 1262, 1474, 1564, 2542\}$ corresponding to $\mathcal{C} = \{-2, -1, 0, 1, 2\}$ respectively. The evolution time we chose to be a time which enables the particle's density profile occupy 80% of the lattice area.

The method to add the noise to our density profiles are different for the data collected in different measurement spaces, i.e. momentum or position. The experimental momentum data measurement can be implemented in cold atom systems as in Ref. [10, 18], where the noise in the data are the shot-noise and Gaussian white noise. The standard deviation of Gaussian noise is set to be 0.02 in our simulated data, which is a reasonable estimation for current technology based on the error bar ranges in Ref. [18]. The experimental position data measurement can be implemented in cold atom system as in Ref. [45] and photonics systems as in Ref. [22, 46] by encoding the position of a walker in either time-bins or spatial modes. The noise in position data includes shot-noise and device noise resulting in the uncertainty in both relative phase and amplitude of the state, which is realised by the convolution between the perfect state and the point-spread function (PSF) of the system. In our noisy data, the PSF we used is a Gaussian with 0 as its mean and 2 as the standard deviation which is also within current experimental techniques level [47, 48].

The configurations of our deep neural network for topological phase identification of quantum systems. We use a deep neural network coupled with an external memory for identification of topological phases from the distributions from CTQWs. We take advantage of the most of up-to-date techniques for our computation network design. For the memory network, the simplification of memory operations is achieved by using a self-organising map (SOM), which is endowed with effective memory addressing and allocation mechanisms. A hybrid learning approach is devised to optimise the network for obtaining promising results.

The detailed architecture and the configuration of our network is illustrated in Fig. 2 and Table II. There are 6 computation blocks (2 with size 8×8, 2 with size 16×16 and 2 with size 32×32), 2 fully connected layers and an external memory. During the training process, the learning rates (LR) for computation network and memory network are 0.0001 and 0.4 respectively. The batch size is set as 64 and the network is trained 1000 iterations. The learning rate decay factor in our computation network is 0.9 for every 100 iterations. The time constant for SOM is the number of iterations divided by the natural logarithm of initial radius (128 in our experiment). The labels for memory clusters are probed by tracking the corresponding coordinates of a few typical data from different topological phases.

Our experiments run on a GPU cluster with three nodes. Each node is with two Intel CPUs of model E5-2680 and 128GB physical memory. For computing acceleration, each CPU manages a separate PCIe slot in which an NVIDIA Quadro P5000 GPU card with 16GB on-board memory installed.

Acknowledgments

This work is supported by the Australian Research Council via the Centre of Excellence in Engineered Quantum Systems project number CE170100009 and Discovery Project numbers DP170103073, DP180100670 and DP180100656. The authors acknowledge discussions about noisy experimental data with Wei Sun, Chao Chen, Yu He, and Steven Flammia, and comments from Robin Harper and John Manion. The authors acknowledge the University of Sydney and University of Technology Sydney for providing HPC resources that have contributed to the research results reported in this paper.

Author Contributions

YM and CL designed and performed experiments. WZ and SB provided theoretical support. WZ prepared the training data. All authors contribute to write the paper.

[1] J. E. Moore, Nature **464**, 194 (2010).
[2] M. Z. Hasan and C. L. Kane, Reviews of Modern Physics **82**, 3045 (2010).
[3] S. Ryu, A. P. Schnyder, A. Furusaki, and A. W. Ludwig, New Journal of Physics **12**, 065010 (2010).
[4] X.-L. Qi and S.-C. Zhang, Reviews of Modern Physics **83**, 1057 (2011).
[5] C. Nayak et al., Reviews of Modern Physics **80**, 1083 (2008).
[6] C. H. Li et al., Nature Nanotechnology **9**, 218 (2014).
[7] Y. Ando et al., Nano Letters **14**, 6226 (2014).
[8] M. DC et al., Nature Materials **17**, 800 (2018).
[9] Quantum Science and Technology, **3**, 045004 (2018).
[10] Z. Wu et al., Science **354**, 83 (2016).
[11] H. M. Price and N. R. Cooper, Physical Review A **85**, 033620 (2012).
[12] L. Duca et al., Science **347**, 288 (2015).
[13] T. Kitagawa, M. S. Rudner, E. Berg, and E. Demler, Physical Review A **82**, 033429 (2010).
[14] T. Kitagawa et al., Nature communications **3**, 882 (2012).
[15] F. Cardano et al., Nature communications **7**, 11439 (2016).
[16] W.-W. Zhang, S. K. Goyal, C. Simon, and B. C. Sanders, Physical Review A **95**, 052351 (2017).
[17] W.-W. Zhang, B. C. Sanders, S. Apers, S. K. Goyal, and D. L. Feder, Physical Review Letters **119**, 197401 (2017).
[18] W. Sun et al., arXiv preprint arXiv:1804.08226 (2018).
[19] X. Zhan et al., Physical Review Letters **119**, 130501 (2017).
[20] S. E. Venegas-Andraca, Quantum Information Processing **11**, 1015 (2012).
[21] E. Flurin et al., Physical Review X **7**, 031023 (2017).
[22] L. Xiao et al., Nature Physics **13**, 1117 (2017).
[23] M. Schmidt and H. Lipson, science **324**, 81 (2009).
[24] A. Krizhevsky, I. Sutskever, and G. E. Hinton, Imagenet classification with deep convolutional neural networks, in *Advances in neural information processing systems*, pages 1097–1105, 2012.
[25] A. Esteva et al., Nature **542**, 115 (2017).
[26] C. J. Shallue and A. Vanderburg, The Astronomical Journal **155**, 94 (2018).
[27] X.-D. Cai et al., Physical Review Letters **114**, 110504 (2015).
[28] M. Schuld, I. Sinayskiy, and F. Petruccione, Contemporary Physics **56**, 172 (2015).
[29] V. Dunjko, J. M. Taylor, and H. J. Briegel, Physical Review Letters **117**, 130501 (2016).
[30] J. Biamonte et al., Nature **549**, 195 (2017).
[31] A. Mott, J. Job, J.-R. Vlimant, D. Lidar, and M. Spiropulu, Nature **550**, 375 (2017).
[32] P. Broecker, J. Carrasquilla, R. G. Melko, and S. Trebst, Scientific reports **7**, 8823 (2017).
[33] J. Carrasquilla and R. G. Melko, Nature Physics **13**, 431 (2017).
[34] P. Zhang, H. Shen, and H. Zhai, Physical Review Letters **120**, 066401 (2018).
[35] K. Choo, G. Carleo, N. Regnault and T. Neupert, Physical Review Letters **121**, 167204 (2018).
[36] S. Lu et al., Physical Review A. **98**, 012315 (2018).
[37] D. Hubel and T. Wiesel, Neuron **75**, 182 (2012).
[38] Y. LeCun, Y. Bengio, and G. Hinton, Nature **521**, 436 (2015).
[39] D. Sticlet, F. Piéchon, J.-N. Fuchs, P. Kalugin, and P. Simon, Physical Review B **85**, 165456 (2012).
[40] J. K. Asbóth, L. Oroszlány, and A. Pályi, Lecture Notes in Physics **919** (2016).
[41] A. Graves et al., Nature **538**, 471 (2016).
[42] N. McLaughlin, J. M. Del Rincon, and P. Miller, Data-augmentation for reducing dataset bias in person re-identification, in *Advanced Video and Signal Based Surveillance (AVSS), 2015 12th IEEE International Conference on*, pages 1–6, IEEE, 2015.
[43] D. Crispell, O. Biris, N. Crosswhite, J. Byrne, and J. L. Mundy, arXiv preprint arXiv:1704.04326 (2017).
[44] T. DeVries and G. W. Taylor, arXiv preprint arXiv:1702.05538 (2017).
[45] C. Robens et al., Optics letters **42**, 1043 (2017).
[46] C. Chen et al., Physical Review Letters **121**, 100502 (2018).
[47] S. Stallinga and B. Rieger, Optical Express **18**, 024461 (2010).
[48] J. Minář et al., Physical Review A **77**, 052325 (2008).

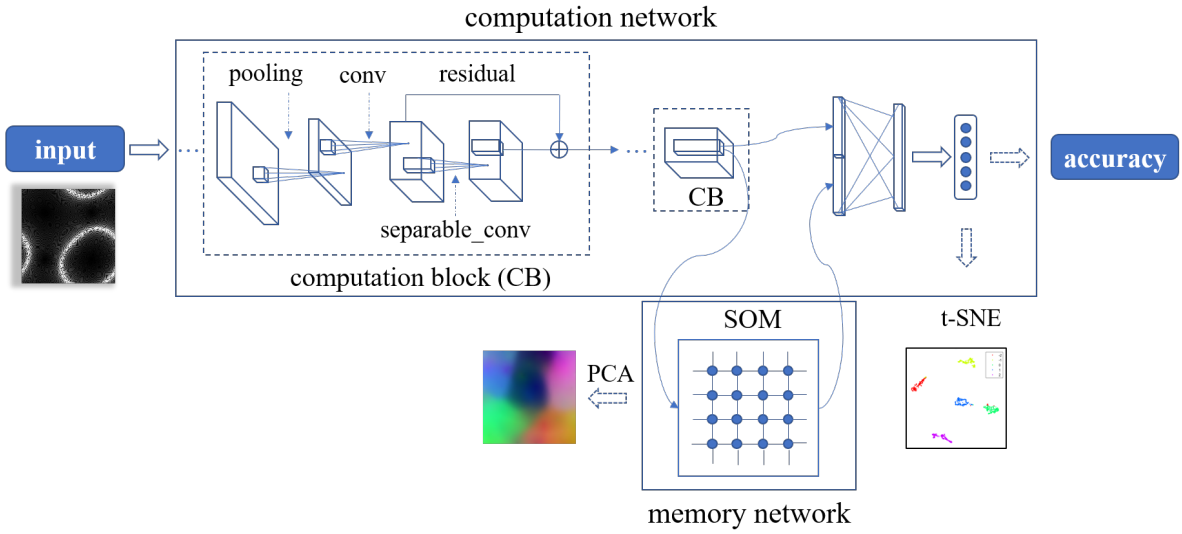

FIG. 2: Network architecture: the computation network is constructed from six computation blocks of a supervised learning paradigm, the memory network is of an unsupervised learning paradigm. "SOM" represents for self-organising map, "conv" represents for convolution. The input of our DNN is the density profiles and the outputs are PCA, t-SNE and statistical accuracy.

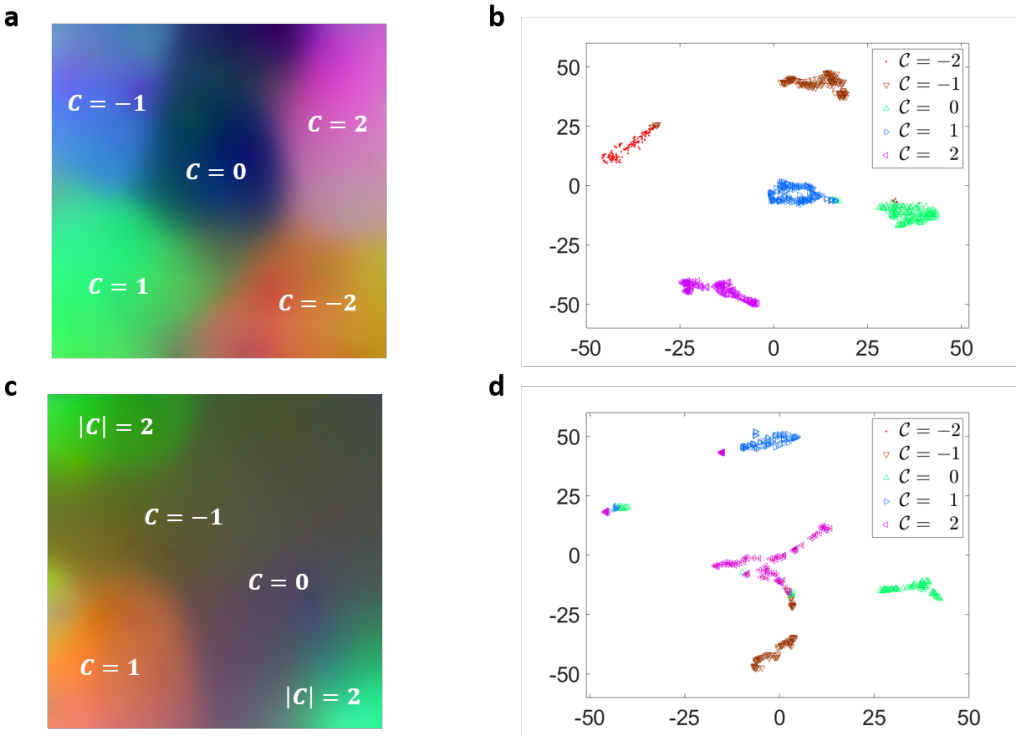

FIG. 3: PCA of memory based on momentum (a) and position (c) density profiles, which illustrate the self-organised clusters formed in memory during our training process and shows the clustering of the input data. The size of PCA is same as the size of the memory in our DNN (256×256). The RGB colour is obtained by projecting the 32 dimensional vector of each memory pixel into a 3 channel colour representation. In our experiments, the scree plots indicate that the first three components explain around 80% of variance, and an "elbow", the cutting-off point, appears at the third principal component. This justifies our choice of first three principal components in our experiments. (b) and (d) are classification visualisations of momentum and position samples via t-SNE, which is a projection from the 5 dimensional DNN output vector into the location indices of a 2 dimensional space.

TABLE I: The statistical accuracy for the topological identification using our DNN. The accuracy is obtained by averaging over three randomised data sets, where every data set is trained three times.

The statistical accuracy with ideal input data							
Density Profile Data		$\mathcal{C}$					Overall
Phase Diagram Area	Measurement Domain	-2	-1	0	1	2	
Whole	Momentum	0.979	0.954	0.965	0.952	1.000	0.970
	Position	0.726	0.961	0.692	0.931	0.195	0.703
Transition	Momentum	0.994	0.869	0.965	0.647	1.000	0.917
	Position	0.94	0.672	0.748	0.587	0.566	0.714
The statistical accuracy with noisy input data							
Density Profile Data		$\mathcal{C}$					Overall
Phase Diagram Area	Measurement Domain	-2	-1	0	1	2	
Whole	Momentum	0.952	0.960	0.955	0.919	1.000	0.957
	Position	0.290	0.955	0.832	0.909	0.554	0.711
Transition	Momentum	0.959	0.880	0.882	0.625	1.000	0.891
	Position	0.924	0.843	0.805	0.648	0.541	0.744

TABLE II: DNN architecture configuration with LR as learning rate.

Computation Network with $LR = 0.0001$						
Block	Layer	Filter	Size	Activation	Padding	Repetition
1st	AvgPool	–	(2,2)	–	Valid	2
	Conv2D	8	(5,5)	–	Valid	
	BatchNorm	–	–	–	–	
	SeparableConv2D	8	(5,5)	ELU	Same	
2nd	AvgPool	–	(2,2)	–	Valid	2
	Conv2D	16	(5,5)	–	Valid	
	BatchNorm	–	–	–	–	
	SeparableConv2D	16	(5,5)	ELU	Same	
3rd	AvgPool	–	(2,2)	–	Valid	2
	Conv2D	32	(5,5)	–	Valid	
	BatchNorm	–	–	–	–	
	SeparableConv2D	32	(5,5)	ELU	Same	
4th	Linear	–	256	Relu	–	1
5th	Linear	–	5	Softmax	–	1
Memory Network with $LR = 0.4$						
Height	Width	Element Size		Decay Factor of LR		Initial Radius
256	256	32		0.9		128